

# DEEM: Diffusion Models Serve as the EyEs of Large Language Models for Image Perception

A PREPRINT

Run Luo<sup>12\*</sup> Yunshui Li<sup>12\*</sup> Longze Chen<sup>12\*</sup> Wanwei He<sup>12</sup> Ting-En Lin<sup>5</sup> Ziqiang Liu<sup>12</sup> Lei Zhang<sup>12</sup>

Zikai Song<sup>6</sup> Xiaobo Xia<sup>4</sup> Tongliang Liu<sup>4</sup> Min Yang<sup>12†</sup> Binyuan Hui<sup>3†</sup>

<sup>1</sup>Shenzhen Institute of Advanced Technology, Chinese Academy of Sciences

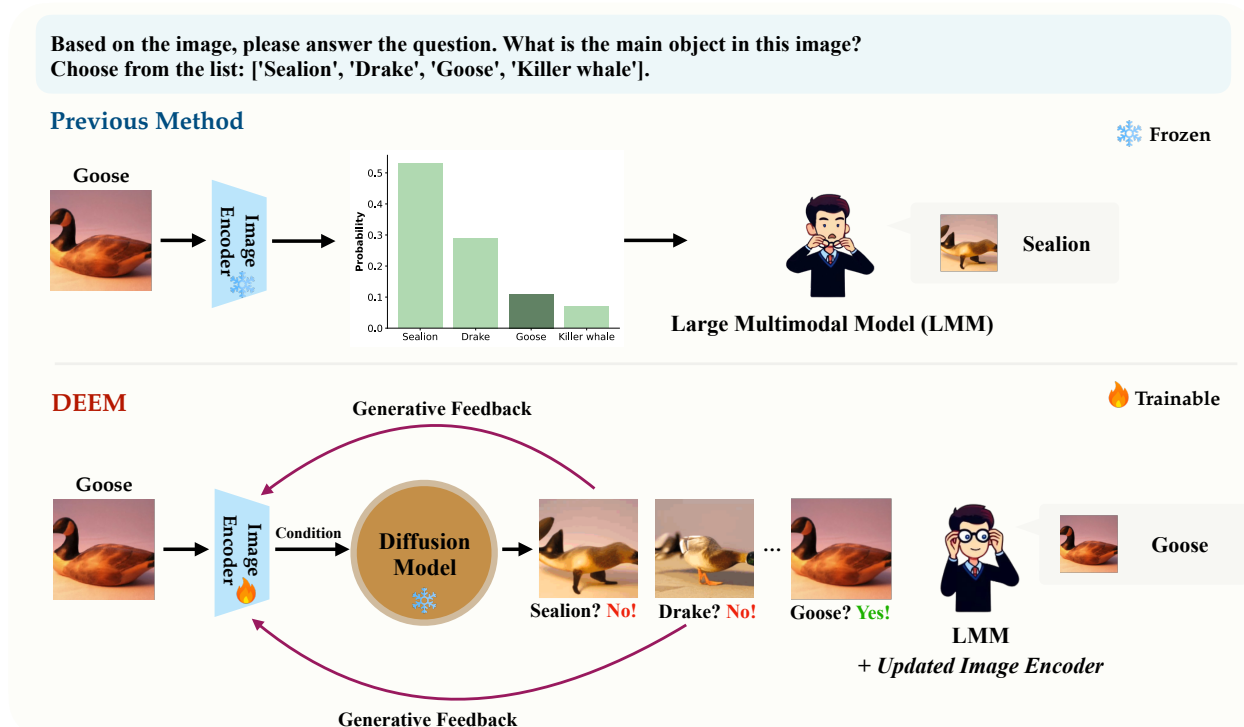
<sup>2</sup>University of Chinese Academy of Sciences

<sup>3</sup>Alibaba Group

<sup>4</sup>The University of Sydney

<sup>5</sup>Tsinghua University

<sup>6</sup>HUST



## ABSTRACT

The development of large language models (LLMs) has significantly advanced the emergence of large multimodal models (LMMs). While LMMs have achieved tremendous success by promoting the synergy between multimodal comprehension and creation, they often face challenges when confronted with out-of-distribution data. This is primarily due to their reliance on image encoders

\*Equal contributions.

†Corresponding authors.

trained to encode images into task-relevant features, which may lead them to disregard irrelevant details. Delving into the modeling capabilities of diffusion models for images naturally prompts the question: Can diffusion models serve as the eyes of large language models for image perception? In this paper, we propose DEEM, a simple and effective approach that utilizes the generative feedback of diffusion models to align the semantic distributions of the image encoder. This addresses the drawbacks of previous methods that solely relied on image encoders like ViT, thereby enhancing the model’s resilience against out-of-distribution samples and reducing visual hallucinations. Importantly, this is achieved without requiring additional training modules and with fewer training parameters. We extensively evaluated DEEM on both our newly constructed RobustVQA benchmark and another well-known benchmark, POPE, for object hallucination. Compared to the state-of-the-art interleaved content generation models, DEEM exhibits enhanced robustness and a superior capacity to alleviate model hallucinations while utilizing fewer trainable parameters, less pre-training data (10%), and a smaller base model size. In particular, DEEM improves the average accuracy on robustness and hallucination evaluation datasets by 24% and 7%, respectively, compared to leading models. Additionally, DEEM can be further enhanced through a supervised fine-tuning phase. Extensive experiments demonstrate the effectiveness of DEEM on various downstream tasks, including visual question answering, image captioning, and text-conditioned image synthesis.

## 1 Introduction

With the success of large language models (LLMs), large multimodal models (LMMs) built on LLMs have garnered significant attention. Researchers [1, 2, 3, 4, 5] have attempted to build a bridge between large language models and image encoders through simple mapping modules, and have already made significant progress in multimodal understanding tasks such as visual question answering. Subsequent studies [6, 7, 8, 9] utilize extra advanced diffusion models (DMs) [10] for image generation and train the LMMs on interleaved text-image data in an end-to-end manner. This unified paradigm of multimodal understanding and creation brings various isolated multimodal tasks together, greatly boosting model capabilities and expanding application scenarios.

However, these models commonly rely on encoder architectures like CLIP-ViT [11] to encode input images. These image encoders are typically trained to encode images into features relevant to downstream tasks, thereby disregarding irrelevant details. Consequently, as shown in Fig. 1, when faced with images outside the training scope, they often capture biased semantic features, resulting in erroneous visual information being perceived by subsequent language models. This accumulation of inaccuracies renders the multimodal model unable to comprehend multimodal context effectively. For this reason, the generated image content lacks the desired level of detail expected by the users.

On the contrary, the goal of diffusion models [12] is to learn a diffusion process that characterizes a probability distribution for a given dataset, without direct training on the downstream task objective. This enables it to capture finer details of images for better handling of out-of-distribution data. However, there have been few efforts to integrate the capabilities of the diffusion model into the image perception of large multimodal models.

In this paper, we propose **DEEM**, a simple and effective approach to leverage the generative feedback of diffusion models for aligning the semantic distributions of image encoders. Building upon this, we introduce an end-to-end interleaved image-text generative modeling approach, where diffusion models serve as additional eyes of large language models for image perception. This addresses the limitations of previous methods that solely relied on image encoders such as CLIP-ViT [11], enhancing the model’s robustness against out-of-distribution samples and reducing hallucination perception in multimodal scenarios, without the need for additional training modules and with fewer training parameters. To the best of our knowledge, we are the first to apply diffusion models to large multimodal models for image perception.

Specifically, DEEM takes interleaved image-text pairs as input to the model. It starts by encoding images and text using corresponding visual and text encoders, resulting in image tokens and text tokens. These tokens are then organized according to their original layout and inputted into a large language model to generate corresponding hidden state outputs. The model employs autoregressive modeling for the hidden state outputs of text and utilizes the output hidden states of images, along with the image tokens encoded by the image encoder, as diffusion conditions. These conditions are then fed into a diffusion model for image reconstruction. Through end-to-end training, the model not only acquires the capacity to generate text and images but also employs semantic consistency regularization on the semantic information produced by the image encoder during image reconstruction. This compels the image encoder to incorporate more details into the semantic representation of the image, thereby mitigating the issue of semantic bias in image encoding.

DEEM is trained on a mixture corpora of image-text pairs and interleaved image-text sequences data without extra in-house data following previous solution [13, 14, 8, 9]. To assess the robustness and hallucination recognition capability of LMMs, we constructed a new robustness benchmark, RobustVQA, based on existing datasets containing natural adversarial samples and out-of-distribution data. RobustVQA is divided into three parts: RobustVQA-A, RobustVQA-R, and RobustVQA-V, based on different data sources, aiming to provide better insights into the performance of LMMs in real-world scenarios. We conducted extensive evaluations of DEEM on both RobustVQA and another widely recognized object hallucination benchmark POPE. Experimental results indicate that our method exhibits enhanced robustness and a superior capacity to alleviate model hallucinations in comparison to the state-of-the-art interleaved image-text modeling model MM-Interleaved [9], using a smaller-scale image encoder (CLIP-ConvNext-B [15] vs. CLIP-ViT-L [11]), a smaller-scale language model (Vicuna 7B vs. Vicuna 13B [16]), and less pre-training data (without Laion-coco [17] & Laion-en [18]). For instance, on RobustVQA-R, DEEM(68.6%) outperforms MM-Interleaved (52.7%), and on POPE-Random, DEEM(69.9%) surpasses MM-Interleaved (64.7%). Moreover, with further enhancement via supervised fine-tuning, DEEM achieves competitive results on various multimodal tasks, including visual question-answering, region-level image captioning, and text-to-image generation.

Before delving into details, we summarize our contributions as follows.

- **Robustness Benchmark.** We design a new robustness benchmark RobustVQA for LMMs based on publicly available ImageNet-A [19], ImageNet-R [20], and ImageNet-V2 [21] datasets, which can be utilized to effectively assess the robustness capabilities of the multimodal models.
- **Effective Method.** We are the first to introduce the diffusion model into the image perception of large language models, to correct potential semantic bias in the image encoder. This approach enhances the model’s robustness and hallucination mitigation capabilities without the need for additional modules or trainable parameters.
- **DEEM Model.** Based on the proposed method, we train a multimodal model with end-to-end interleaved text-image modeling capabilities. After supervised fine-tuning, DEEM can perform various multimodal tasks in a unified manner, such as visual question answering, text-to-image generation, and region-level image captioning.
- **Comprehensive Experiments.** We provide abundant qualitative and quantitative comprehensive experimental results to demonstrate the effectiveness and efficiency of the proposed method.

## 2 Related Work

### 2.1 LMM for Text Generation Only

Image-to-text large multimodal models (LMMs) inject visual information into large language models (LLMs) through vision foundation models (VFMs), allowing the language models to perceive visual inputs and thus generate captions or answer questions based on the given multimodal content. Flamingo [4] tries to extract vision features with a resampler, and transfer them into the text features with a cross-attention mechanism. Instead of using cross-attention layers, BLIP-2 [14] directly feed the visual features into the LLMs as soft prompts and significantly reduce the training cost by reducing the visual token number. LLaVa [1] and MiniGPT-4 [2] construct a small-scale instruction tuning dataset to better align the LMM with the expected output format. However, these LMMs are limited to holistic image understanding without the ability to conduct region-level reasoning. In order to accept the region as input, GPT4ROI [22] proposes to encode the regions as features. Kosmos-2 [23] introduces additional location tokens to the LLM’s vocabulary for either coordinates input or output. Shikra [5] turns the box coordinates into normalized numerical values with certain precision without retraining the LLM’s original vocabulary. Although this unidirectional image-to-text paradigm has achieved tremendous success, it still fails to unify multimodal tasks like text-to-image generation and image-to-text visual question answering, significantly limiting the capabilities of multimodal models.

### 2.2 LMM for Image and Text Generation

In order to unify multimodal tasks into a unified manner, some works [6, 24, 7, 8, 9] attempt to generate images and text in the interleaved context concurrently. The release of some public large-scale interleaved image-text datasets [25, 26] has significantly advanced the development of this field. CM3Leon [6] converts images into discrete tokens, facilitating token-level auto-regressive modeling as traditional language modeling. Although CM3Leon showcases competitive image generation capabilities, it exhibits notable weaknesses in image understanding. Emu [7] and DreamLLM [8] focus on single-stage end-to-end modeling using raw image pixels as input for interleaved image-text generation modeling, but they feed image information at the input of LMMs, which are limited by the problem that fixed number of visual tokens cannot efficiently describe image details.

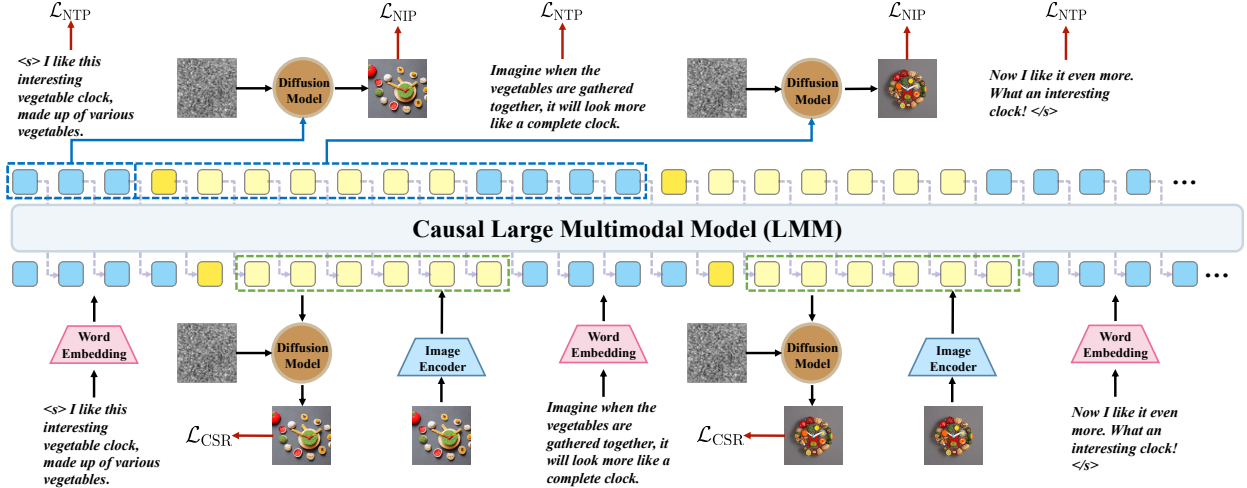


Figure 2: **Overview of our DEEM framework.** Interleaved documents serve as input, decoded to produce outputs. Both text and images are encoded into sequential, discrete token embeddings for the LMM input. The text is predicted in an autoregressive manner and the images are synthesized by the DM-based image decoder conditioned on holistic historical semantics captured by LMM. Besides, the image token embeddings are fed into DM-based image decoder for consistent image restoration.

MM-Interleaved [9], a concurrent SOTA open-source model for end-to-end interleaved image-text generation modeling, addresses this limitation by integrating image details into LMMs via multi-scale visual features. However, when faced with out-of-distribution noisy data, the image encoders used by LMMs often produce incorrect visual information, ultimately leading to erroneous predictions. This significantly limits the application of the models in safety-critical scenarios. Building on an advanced interleaved content modeling mechanism, we propose DEEM, which cleverly reuses DMs to correct the outputs of the VFMs without increasing extra parameter count, thereby enhancing the model’s generalization capabilities and reducing visual hallucinations. Similar to previous work [1, 8, 9], after supervised fine-tuning, it achieves competitive performance on multiple downstream multi-modal tasks with the smallest scale.

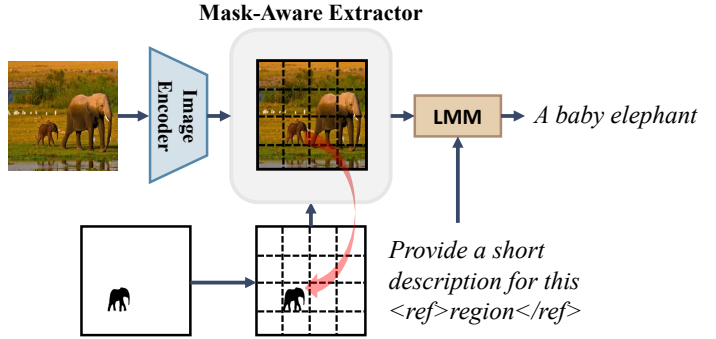


Figure 3: **Pipeline of Mask-Aware Extractor.** The mask-aware extractor can be used to extract region-level visual features based on the mask-aware operation.

### 3 Method

In this section, we first present our DEEM, starting with an introduction to the overall architecture in Section 3.1, followed by a description of the pipeline in Section 3.2. Finally, we provide details on the training and inference process in Section 3.3.

#### 3.1 Architecture

In this subsection, we present the multi-modal architecture for processing interleaved image-text data. To excel in both comprehension and creation tasks of text and images, a multi-modal model consists of the following three key components.

**VFM-based Image Encoder**  $\mathcal{E}_V$  which encodes each image  $x^V \in \mathbb{R}^{H \times W \times 3}$  into an image embedding  $e^V \in \mathbb{R}^{N \times C}$ , where  $C$  is the channel dimension and  $N$  is the number of visual tokens in image embedding. **LLM-based Multi-modal Decoder**  $\mathcal{D}_{LLM}$  that extracts context features from the interleaved image-text token sequences. Its input sequence  $E \in \mathbb{R}^{K \times C}$  is a concatenation of embeddings  $(e_1, e_2, \dots)$ , where  $e_n$  is either a word embedding  $e_n^L \in \mathbb{R}^{1 \times C}$  or an image embedding  $e_n^V \in \mathbb{R}^{N \times C}$ .  $K$  is the total number of input tokens. **DM-based Image Decoder**  $\mathcal{D}_{DM}$  that generates the image conditioned on image-text sequences context feature.

To provide the conditional inputs for  $\mathcal{D}_{DM}$  and reduce the number of visual tokens in image embedding  $e^V$ , two different Perceiver Resampler [4] are employed to map the output features from multi-modal decoder  $\mathcal{D}_{LLM}$  and image encoder  $\mathcal{E}_V$  to a fixed number of conditional tokens, respectively. Additionally, we utilize an extra mask-aware visual extractor  $\mathcal{E}_M$  for extracting region visual information from image embedding  $e^V$  via simple mask-aware operation  $\mathcal{E}_M(e^V, \mathcal{M}^V)$ , where  $\mathcal{M}^V$  is the corresponding binary mask of image  $x^V$ .

### 3.2 Pipeline

As shown in Fig. 2, given an interleaved image-text sequence  $X = \{x_1, x_2, x_3, \dots\}$ , where each element  $x_n$  is either a text token (denoted as  $x_n^L$ ) or a whole image (denoted as  $x_n^V$ ). Text and images are arranged in the order in which they appear in the original content. To build an end-to-end generative model for interleaved image-text data, a common practice is to first extract embedding for each text token and each image and then feed them into LLMs, *i.e.*,  $e_n^L = \mathcal{E}_L(x_n^L)$  and  $e_n^V = \mathcal{E}_M(\mathcal{E}_V(x_n^V), \mathcal{M}_n^V)$ , where  $\mathcal{E}_L$  denotes word embedding in LLM.  $\mathcal{E}_V$  is typically an image encoder followed by a Perceiver Resampler [4] to map each image to a fixed number of visual tokens. As shown in Fig. 3, we introduce a mask-aware visual extractor  $\mathcal{E}_M$  for extracting region visual information from image embedding  $e_n^V$  via simple mask-aware operation  $\mathcal{E}_M(e_n^V, \mathcal{M}_n^V)$ , where  $\mathcal{M}_n^V$  is the corresponding binary mask of image  $x_n^V$  and the default value is 1. Then, the interleaved generative modeling is trained to maximize the log-likelihood:

$$\log p(X) = \sum_n \log p(x_n | e_{<n}) = \sum_{n \in \mathcal{I}_L} \underbrace{\log p(x_n^L | e_{<n})}_{\text{text prediction}} + \sum_{n \in \mathcal{I}_V} \underbrace{\log p(x_n^V | e_{<n})}_{\text{image prediction}}, \quad (1)$$

where  $\mathcal{I}_L$  and  $\mathcal{I}_V$  represent the index sets for text tokens and images, respectively. That  $<n$  in the subscript represents the abbreviation of  $\{1, 2, \dots, n-1\}$ . The following paragraphs provide explanations of Eq. (1).

**Text Generation with Multi-modal Condition.**  $\log p(x_n^L | e_{<n})$  is similar to traditional causal language modeling, except that the condition also includes previous images. Recent works [4, 14, 1] have demonstrated the effectiveness of using LLMs for processing additional visual inputs. The loss function for text generation is

$$\mathcal{L}_{NTP}(x_n^L | e_{<n}) = -\log p(x_n^L | \mathcal{D}_{LLM}(e_{<n})), \quad (2)$$

where  $\mathcal{D}_{LLM}$  denotes the LLM network.

**Image Generation with Multi-modal Condition.** Maximizing  $\log p(x_n^V | e_{<n})$  aligns with the diffusion denoising process, which recently achieved widespread success in image generation. Maximizing the log-likelihood is derived as minimizing the diffusion modeling loss as

$$\mathcal{L}_{NIP}(x_n^V | e_{<n}) = \mathbb{E}_{\epsilon, t} \|\epsilon - \mathcal{D}_{DM}(x_{n,t}^V, t, \mathcal{D}_{LLM}(e_{<n}))\|^2, \quad (3)$$

where  $\mathcal{D}_{DM}$  is the diffusion model for denoising process. That  $x_{n,t}^V$  is the noisy version of the original image at the denoising step  $t$ , and the denoising network  $\mathcal{D}_{DM}$  is trained to predict the noise  $\epsilon$ .

**Consistency Semantic Regularization.** In addition to the above text and image generation loss functions, we propose a new consistency semantic constraint term. This term reuses the diffusion model to perform generative checks on the image semantic information extracted by the image encoder, ultimately correcting erroneous knowledge in the pre-trained image encoder. This significantly enhances the out-of-distribution generalization and reduces visual hallucinations in the multi-modal model. The new log-likelihood function can be written as

$$\log p^*(X) = \sum_{n \in \mathcal{I}_L} \underbrace{\log p(x_n^L | e_{<n})}_{\text{text prediction}} + \sum_{n \in \mathcal{I}_V} \underbrace{\log p(x_n^V | e_{<n})}_{\text{image prediction}} + \sum_{n \in \mathcal{I}_V} \underbrace{\log p(x_n^V | e_n)}_{\text{image restoration}}. \quad (4)$$

Similarly, the corresponding log-likelihood function  $\log p(x_n^V | e_n)$  can be equivalently written as the following loss function used in training:

$$\mathcal{L}_{CSR}(x_n^V | e_n) = \mathbb{E}_{\epsilon, t} \|\epsilon - \mathcal{D}_{DM}(x_{n,t}^V, t, e_n)\|^2. \quad (5)$$

Note that the new end-to-end modeling framework brings significant improvements to the generalization performance of the model without altering the original modeling flexibility or introducing additional modules.

### 3.3 Training and Inference

We employ a three-stage training process, consisting of image-text alignment pre-training, image-text instruction fine-tuning, and mask-text instruction fine-tuning. The image-text alignment pre-training objective is defined as the sum of the next-text prediction loss in Eq. (2), next-image prediction loss in Eq. (3) and consistency semantic regularization

Table 1: **Zero-shot visual robustness and hallucination evaluation** of RobustVQA-A, RobustVQA-R, RobustVQA-V, POPE-Random: POPE-R [27], POPE-Popular: POPE-P [27], and POPE-Adversarial: POPE-A [27] benchmarks. RobustVQA-A, RobustVQA-R, and RobustVQA-V are robustness benchmarks designed by us in Appendix D.1. "AVG" denotes the overall average accuracy of six benchmarks. "SFT" denotes the supervised fine-tuning. "Param" denotes trainable parameters. The evaluation metrics for each benchmark are listed in Table 12.

Method	Param	SFT	Architecture	RobustVQA-A	RobustVQA-R	RobustVQA-V	POPE-R	POPE-P	POPE-A	AVG
<i>Models for both Image and Text Retrieval</i>										
CLIP	-	✗	RN18	1.41	34.64	57.13	-	-	-	31.06
	-	✗	ViT-B	9.01	45.23	61.04	-	-	-	38.43
	-	✗	ConvNext-B	22.73	47.82	62.34	-	-	-	44.30
<i>Models for Text Generation Only</i>										
LLaVa [1]	~ 13 B	✓	ViT-L/Vicuna 13B	54.82	59.99	58.37	50.37	49.87	49.70	53.84
Shikra [5]	~ 7 B	✓	ViT-L/LLaMA 7B	33.71	38.33	37.45	86.90	83.97	<b>83.10</b>	60.58
NeXt-Chat [28]	~ 7 B	✓	ViT-L/Vicuna 7B	44.82	43.67	47.30	<b>87.70</b>	<b>84.57</b>	81.93	64.99
<i>Models for both Image and Text Generation</i>										
MM-Interleaved [9]	1465.2 M	✗	ViT-L/Vicuna 13B	50.76	52.71	50.60	64.73	65.33	65.20	58.22
Baseline	1271.0 M	✗	ConvNext-B/Vicuna 7B	53.24	56.06	54.72	50.55	52.00	51.93	53.08
DEEM(Ours)	494.9 M	✗	ConvNext-B/Vicuna 7B	<b>56.86</b>	<b>68.63</b>	<b>63.08</b>	69.93	70.27	68.87	66.27
DEEM-VQA (Ours)	~ 7 B	✓	ConvNext-B/Vicuna 7B	53.12	62.99	61.22	87.40	82.80	78.49	<b>71.00</b>

loss in Eq. (5) as  $\mathcal{L}_{S_1} = \mathcal{L}_{NTP} + \lambda \mathcal{L}_{NIP} + \lambda \mathcal{L}_{CSR}$ , where  $\lambda$  is a coefficient used to determine the relative loss weight between the image and text decoding branches. In order to enable the DEEMto perform general multimodal comprehension and creative tasks following human instructions, we use  $\mathcal{L}_{S_2} = \mathcal{L}_{NTP} + \lambda \mathcal{L}_{CSR}$  to conduct image-text instruction fine-tuning. To further enhance the model’s fine-grained region awareness, we conducted region-level mask-text instruction fine-tuning. Since there is no need to perform text-to-image tasks, we removed the next-image prediction loss and the training objective in mask-text instruction fine-tuning can be defined as  $\mathcal{L}_{S_3} = \mathcal{L}_{NTP}$ . The whole framework can be optimized end-to-end during the three stages. During inference, the images and texts are generated in an auto-regressive manner. Text tokens are sampled from the distribution predicted by the multi-modal LLM. When the generated token is <SoI>, the diffusion model is called for generating the next image.

## 4 Experiment

### 4.1 Implementation Details

In this subsection, we first introduce the network of DEEMand then showcase the three-stage training recipes. More details of datasets and hyper-parameters can be found in Table 11.

**Network.** Similar to previous work, We leverage Vicuna7B [16] and Stable Diffusion v2.1 [10] as the large language model, and image decoder, respectively. However, unlike their use of a 427M parameter CLIP-ViT-L as the image encoder, we use a smaller 122M parameter CLIP-ConvNeXt-B[15]. For the multi-modal LLM, a Perceiver Resampler [4] with 12 blocks is used to reduce the number of visual tokens per image to 77.

**Image-Text Alignment Pre-training.** Our model is pre-trained on a mixture of image-text pairs and interleaved image-text sequences, including MMC4-Core [26], LAION-400M [29], SBU [30], and CC-12M [31]. For LAION-400M [29], SBU [30], and CC-12M [31], instead of utilizing the original annotations, we use the version filtered by the pre-trained BLIP-2 model [14]. For simplicity, we refer to it as BLIP-LCS hereafter. "LCS" abbreviates the LAION, CC, and SBU datasets. The sampling probability of MMC4 is twice that of BLIP-LCS. The images are inserted before or after the corresponding text sentence with equal probability. To optimize training efficiency and data utility, multiple image-text pairs or interleaved image-text sequences are concatenated into extended sequences with the maximum context length.

**Image-Text Instruction Fine-tuning.** To enable DEEMto perform general multimodal comprehension tasks following human instructions, we utilize publicly available datasets for image-text instruction fine-tuning, including LLaVA-665K [1], COCO Caption [32], VQAv2 [33],TextCaps [34], OCR-VQA [35], GQA [36], OK-VQA [37], TextVQA [38], and AOK-VQA [39].



Figure 4: **Examples from ImageNet-R, ImageNet-A, and ImageNet-V2.** These examples share similar backgrounds, rare materials, and unusual textures. They serve as natural adversarial examples and out-of-distribution data, which can be used to test the robustness of models.

Table 2: **Multi-modal comprehension evaluation.** “ED” denotes using extra in-house data. Benchmarks include COCO [32]; I2Para.: Image2Paragraph [46]; VQA<sup>v2</sup>: VQAv2 [33]; OKVQA [37]; GQA [36]; VizWiz [47]; VisDial [48]. The evaluation metrics for each benchmark are listed in Table 12.

Model	LLM	VFM	ED	COCO	I2Para.	VQA <sup>v2</sup>	OKVQA	GQA	VizWiz	VisDial
<i>Models for Text-Generation Only</i>										
IDEFICS-80B [49]	LLaMA-65B	ViT-H	✗	91.8	–	60.0	–	45.2	36.0	–
IDEFICS-80B-I [49]	LLaMA-65B	ViT-H	✗	117.2	–	37.4	–	–	26.0	–
KOSMOS-1 [50]	MetaLM	ViT-L	✓	–	–	46.7	–	–	–	–
KOSMOS-2 [23]	KOSMOS-1	ViT-L	✓	–	–	45.6	–	–	–	–
Flamingo-9B [4]	Chinchilla-7B	ViT-L	✓	79.4	–	51.8	44.7	–	28.8	48.0
Flamingo-80B [4]	Chinchilla-70B	ViT-H	✓	84.3	–	56.3	50.6	–	31.6	52.0
mPLUG-DocOwl [51]	LLaMA-7B	ViT-L	✗	52.6	–	–	–	–	–	–
BLIP-2 [14]	Vicuna-7B	ViT-L	✗	–	–	–	–	38.6	25.3	–
BLIP-2 [14]	Vicuna-13B	ViT-L	✗	–	–	41.0	–	41.0	19.6	–
InstructBLIP [?]	Vicuna-7B	ViT-L	✗	–	–	–	–	49.2	34.5	–
InstructBLIP [3]	Vicuna-13B	ViT-L	✗	–	–	–	–	49.5	33.4	–
Shikra [5]	Vicuna-13B	ViT-L	✗	117.5	–	77.4	–	–	–	–
LLaVA-1.5 [52]	Vicuna-7B	ViT-L	✗	–	–	78.5	–	62.0	50.0	–
LLaVA-1.5 [52]	Vicuna-13B	ViT-L	✗	–	–	80.0	–	63.3	53.6	–
Qwen-VL [53]	Qwen-7B	ViT-G	✓	–	–	78.8	–	59.3	35.2	–
Qwen-VL-Chat [53]	Qwen-7B	ViT-G	✓	–	–	78.2	–	57.5	38.9	–
<i>Models for both Image and Text Generation</i>										
CM3Leon [6]	–	–	✓	61.6	10.5	47.6	23.8	–	37.6	22.6
Emu [7]	Vicuna-13B	ViT-L	✓	112.4	–	52.0	38.2	–	34.2	47.4
Emu-I [7]	Vicuna-13B	ViT-L	✓	117.7	–	40.0	34.7	–	35.4	48.0
Emu2 [54]	LLaMA-33B	ViT-L	✓	–	–	33.3	26.7	–	40.4	–
MM-Interleaved [9]	Vicuna-13B	ViT-L	✗	129.0	23.5	57.0	40.0	46.7	40.8	48.7
DreamLLM [8]	Vicuna-7B	ViT-L	✗	115.4	17.4	56.6	44.3	–	38.1	–
DEEM-VQA	Vicuna-7B	ConvNext-B	✗	115.4	22.4	68.2	53.4	55.7	50.4	42.1

**Mask-Text Instruction Fine-tuning.** At this stage, we use a simple mask-aware visual extractor to capture pixel-level region features and then align mask-based region features with language embeddings. We collect short text and pixel-level mask pairs from the publicly available object-level datasets (COCO [32], RefCOCO [40], RefCOCO+ [41], RefCOCOg [41]), part-level datasets (Pascal Part [42], Part Imagenet [43]), and multiple region datasets (VCR [44], Visual Genome [45]). Then we conduct mask-text instruction fine-tuning on the mixture of the above text-mask pairs data, enabling DEEM to complete region-level understanding tasks, such as region-level image captioning.

## 4.2 Experimental Results

In this study, we evaluate our DEEM model by comparing it with current state-of-the-art (SOTA) models on various tasks including visual robustness and hallucination diagnosis, region-level image captioning, image-level visual question answering, and text-to-image generation. All metrics and data splits are listed in Table 11 in Appendix D.

**Visual Robustness and Hallucination Diagnose.** To rigorously assess the neural networks robustness of our model, we design a benchmark called RobustVQA for robustness evaluation based on online datasets, including ImageNet-A [19], ImageNet-R [20] and ImageNet-V2 [21]. As shown in Fig. 4, these challenging natural adversarial examples and out-of-distribution samples in the original ImageNet dataset can be used to evaluate the neural network robustness of our model. Similar to the POPE dataset, we first convert the original ImageNet-A, ImageNet-R, and ImageNet-V2 data into a VQA format that the multimodal model can evaluate simply. More details about the new benchmark RobustVQA design can be found in Appendix D.1. For a comprehensive visual robustness and hallucination evaluation, we evaluate our model against other open-source state-of-the-art (SOTA) LMMs, including LLaVA [1], Shikra [5], MM-Interleaved [9], and NeXt-Chat [28], on the RobustVQA and POPE [27] dataset with accuracy metric. The results, presented in Table 1, demonstrate that our DEEM model not only exhibits competitive performance compared with existing fine-tuned SOTA models on POPE after fine-tuning, but also

Table 3: **Zero-shot region-level image captioning results** on ReferCOCOg.

Method	Type	METEOR	CIDEr
GRIT [55]	Box	15.2	71.6
Kosmos-2 (0-shot) [23]	Box	12.2	60.3
Kosmos-2 (2-shot) [23]	Box	13.8	62.2
Kosmos-2 (4-shot) [23]	Box	14.1	62.3
NeXt-Chat [28]	Box	12.0	79.0
DEEM-Mask	Mask	14.1	71.0

achieves the best results among visual robustness benchmark only after pre-training. Notably, compared to the larger-scale concurrent SOTA model for interleaved text-image modeling, MM-Interleaved [9], our model achieves better results in visual hallucination and robustness experiments with a smaller scale. Our model obtains an average 11.5 absolute accuracy gain on the robustness benchmark and an average 4.6 absolute accuracy gain on the hallucination benchmark, respectively. To ensure a fair comparison and prove the effectiveness of our method, we also train an MM-Interleaved model with the same experimental setting as a baseline. Compared to this baseline, Our method achieves an average 4.4 absolute accuracy gain on the robustness benchmark and an average 18.1 absolute accuracy gain on the hallucination benchmark, respectively. The experimental results demonstrate the effectiveness of incorporating consistency language regularization in our method.

### Image-Level Visual Question Answering and Captioning.

In order to assess multimodal vision and language capabilities of DEEM, we conduct evaluation against current SOTA LMMs including LLaVA-1.5 [52], Qwen-VL [53], DreamLLM [8] and MM-Interleaved [9] across several tasks, including image captioning on COCO [32], Image2Paragraph [46], visual question answering on VQAv2 [33], OKVQA [37], GQA [36], VizWiz [47], and VisDial [48]. As demonstrated in Table 2, DEEM exhibits superior or comparable performance relative to SOTA models. In comparison with models for text generation only, our approach consistently achieves competitive performance across various dataset splits. Against models for both image and text generation, DEEM demonstrates enhanced performance in seven dataset splits, notably achieving a substantial 5.0-point improvement in Image2Paragraph [46]. It is noteworthy that DEEM is trained with a significantly smaller image encoder CLIP-ConvNeXt-B [15], comprising only 122M parameters, in stark contrast to baselines such as DreamLLM [8], which utilize larger 427M CLIP-ViT-L [11]. These results indicate that our method can enhance the model’s robustness performance without compromising the multimodal vision and language capabilities of our model.

**Region-Level Image Captioning.** In addition to holistic image understanding, we also validate the model’s ability to take region-level image captioning. As shown in Fig. 3, we use a mask-aware extractor to obtain region-level visual features and address region-level image captioning tasks. We adopt the RefCOCOg [41] validation set and compare it with other state-of-the-art (SOTA) models, including GRIT [55], Kosmos-2 [23], and NeXt-Chat [28]. The CIDEr [66] and METEOR are applied as the evaluation metrics. As shown in Table 3, our model is capable of achieving competitive performance on CIDEr and METEOR across all of the compared methods, which shows the superiority of our DEEM.

**Text-to-Image Generation.** we evaluate text-conditional image generation on MS-COCO [67] and LN-COCO [68]. On MSCOCO, we sample 8 images per text condition and use CLIP-ViT-L [11] to rerank based on text-image similarity. CLIP reranking is not used for LN-COCO. FID [69] is used to evaluate both datasets. As shown in Table 4, our model shows competitive text-to-image generation compared to existing image and text generation models. See qualitative results on text-to-image synthesis in Fig. 9 in Appendix E.

### 4.3 Ablation Study

In this study, we conduct ablation studies on several key components of the model, including consistency semantic regularization, training latency, and the impact of image resolution. Benchmarks include RobustVQA-A:RVQA-A; RobustVQA-R: RVQA-R; RobustVQA-V:RVQA-V; POPE-R [27]; POPE-P [27]; POPE-A [27]. More additional ablation studies can be found in Appendix C.

Table 5: Ablation study of consistency semantic regularization loss  $\mathcal{L}_{CSR}$  in image-text alignment pre-training with 10k training steps and 128 batch size.

$\mathcal{L}_{CSR}$	RVQA-A	RVQA-R	RVQA-V	POPE-R	POPE-P	POPE-A
✗	53.2	56.1	54.7	50.6	52.0	51.9
✓	<b>57.8</b>	<b>69.0</b>	<b>64.8</b>	<b>69.9</b>	<b>70.3</b>	<b>68.9</b>

Table 4: **Zero-shot text-to-image generation FID** on MS-COCO and LN-COCO.

Method	MS-COCO	LN-COCO
<i>Text-to-Image Specialists</i>		
Retrieval Result	17.97	33.59
DALL-E [56]	~28	-
CogView [57]	27.10	-
CogView2 [58]	24.00	-
Stable Diffusion [10]	12.43	34.26
GLIDE [59]	12.24	-
Make-A-Scene [60]	11.84	-
DALL-E 2 [61]	10.39	-
Muse-3B [62]	7.88	-
Imagen-3.4B [63]	7.27	-
Parti-20B [64]	7.23	15.97
<i>Models for both Image and Text Generation</i>		
CM3-13B [65]	29.56	-
GILL-8B [24]	12.25	-
Emu-13B [7]	11.66	-
CM3Leon-7B [6]	10.82	-
DreamLLM-7B [8]	8.76	22.42
MM-Interleaved-13B [9]	7.90	23.88
DEEM-7B (Ours)	8.89	24.13

Table 6: Ablation study of consistency semantic regularization loss  $\mathcal{L}_{CSR}$  in image-text instruction fine-tuning with 2k training steps and 16 batch size.

$\mathcal{L}_{CSR}$	RVQA-A	RVQA-R	RVQA-V	POPE-R	POPE-P	POE-A
✗	51.3	56.5	57.4	85.4	78.8	76.2
✓	<b>53.5</b>	<b>57.6</b>	<b>58.1</b>	<b>86.0</b>	<b>79.2</b>	<b>77.1</b>



**Consistency Semantic Regularization.** To evaluate the effectiveness of the key elements of our design, we conduct the following ablation experiments. We first pre-train a baseline model without using the consistency semantic regularization term under the same training setting for comparison to demonstrate the effectiveness of our architecture. As we can see from Table 5, during the pre-training phase, using our consistency semantic regularization can significantly enhance the model’s performance on both hallucination and robustness benchmarks. Moreover, we load the weights of the pre-trained model for image-text instruction fine-tuning experiments. In the second phase of image-text instruction fine-tuning experiments, we demonstrate the effectiveness of our model design. As shown in Table 6, we observe that after fine-tuning with image-text instruction data, the model’s visual hallucination ability improves further, but its visual perception robustness decreases. However, using our consistency semantic regularization can mitigate the robustness degradation while further enhancing the model’s visual hallucination ability.

**Ablation Study of Training Latency** To explore the impact of introducing consistency semantic regularization on the training latency in the two stages of training, we conduct corresponding ablation experiments. As shown in the Table 7, using the consistency semantic regularization introduces approximately 14% and 4% additional training latency in the first and second stages of training, respectively. In the two stage, since we utilize the DM-based image decoder one more time than the baseline during training, the introduction of the consistency regularization term leads to more additional training latency. However, this simple yet effective method significantly enhances the model’s robustness capabilities with fewer trainable parameters compared to the baseline after the first stage of training.

Table 7: Ablation study of training latency in Image-Text Alignment Pre-training and Image-Text Instruction Fine-tuning stage.

phase	DEEM	Baseline
stage1	9.25 s/step	8.11 s/step
stage2	2.22 s/step	2.14 s/step

## 5 Conclusion

Can diffusion models serve as the eyes of large language models for image perception? In this paper, we answer the question by proposing a novel method called DEEM, which leverages a diffusion model as the eyes for LLMs. This approach enhances the robustness of the multimodal model for interleaved image-text modeling and reduces visual hallucinations without introducing extra modules. Through comprehensive exploratory experiments, we demonstrate the effectiveness of the proposed DEEM method. In addition to its advanced robust performance and visual hallucination handling capabilities, we adopt an additional two-stage instruction fine-tuning process to broaden the application scenarios of our DEEM. This enables DEEM to handle a variety of multimodal tasks, including visual question answering, image captioning, and region-level image reasoning. Besides, this work initiates the first step towards visual robustness via generative feedback in a multimodal model. In the future, we will continue to enhance the model’s ability to conduct better multimodal comprehension and creation tasks. As an end-to-end framework, we hope it will spur further research in the multimodal robustness field, such as multimodal agents that can handle complex tasks that require safety abilities.

## References

- [1] Haotian Liu, Chunyuan Li, Qingyang Wu, and Yong Jae Lee. Visual instruction tuning. In *NeurIPS*, 2024.
- [2] Deyao Zhu, Jun Chen, Xiaoqian Shen, Xiang Li, and Mohamed Elhoseiny. Minigt-4: Enhancing vision-language understanding with advanced large language models. *arXiv preprint arXiv:2304.10592*, 2023.
- [3] Wenliang Dai, Junnan Li, Dongxu Li, Anthony Meng Huat Tiong, Junqi Zhao, Weisheng Wang, Boyang Li, Pascale N Fung, and Steven Hoi. Instructblip: Towards general-purpose vision-language models with instruction tuning. In *NeurIPS*, 2024.
- [4] Jean-Baptiste Alayrac, Jeff Donahue, Pauline Luc, Antoine Miech, Iain Barr, Yana Hasson, Karel Lenc, Arthur Mensch, Katherine Millican, Malcolm Reynolds, et al. Flamingo: a visual language model for few-shot learning. In *NeurIPS*, pages 23716–23736, 2022.
- [5] Keqin Chen, Zhao Zhang, Weili Zeng, Richong Zhang, Feng Zhu, and Rui Zhao. Shikra: Unleashing multimodal llm’s referential dialogue magic. *arXiv preprint arXiv:2306.15195*, 2023.
- [6] Lili Yu, Bowen Shi, Ramakanth Pasunuru, Benjamin Muller, Olga Golovneva, Tianlu Wang, Arun Babu, Binh Tang, Brian Karrer, Shelly Sheynin, et al. Scaling autoregressive multi-modal models: Pretraining and instruction tuning. *arXiv preprint arXiv:2309.02591*, 2(3), 2023.
- [7] Quan Sun, Qiyang Yu, Yufeng Cui, Fan Zhang, Xiaosong Zhang, Yueze Wang, Hongcheng Gao, Jingjing Liu, Tiejun Huang, and Xinlong Wang. Emu: Generative pretraining in multimodality. In *ICLR*, 2023.
- [8] Runpei Dong, Chunrui Han, Yuang Peng, Zekun Qi, Zheng Ge, Jinrong Yang, Liang Zhao, Jianjian Sun, Hongyu Zhou, Haoran Wei, et al. Dreamllm: Synergistic multimodal comprehension and creation. *arXiv preprint arXiv:2309.11499*, 2023.
- [9] Changyao Tian, Xizhou Zhu, Yuwen Xiong, Weiyun Wang, Zhe Chen, Wenhai Wang, Yuntao Chen, Lewei Lu, Tong Lu, Jie Zhou, et al. Mm-interleaved: Interleaved image-text generative modeling via multi-modal feature synchronizer. *arXiv preprint arXiv:2401.10208*, 2024.
- [10] Robin Rombach, Andreas Blattmann, Dominik Lorenz, Patrick Esser, and Björn Ommer. High-resolution image synthesis with latent diffusion models. In *CVPR*, pages 10684–10695, 2022.
- [11] Alec Radford, Jong Wook Kim, Chris Hallacy, Aditya Ramesh, Gabriel Goh, Sandhini Agarwal, Girish Sastry, Amanda Askell, Pamela Mishkin, Jack Clark, et al. Learning transferable visual models from natural language supervision. In *ICML*, pages 8748–8763, 2021.
- [12] Jonathan Ho, Ajay Jain, and Pieter Abbeel. Denoising diffusion probabilistic models. In *NeurIPS*, pages 6840–6851, 2020.
- [13] Junnan Li, Dongxu Li, Caiming Xiong, and Steven Hoi. Blip: Bootstrapping language-image pre-training for unified vision-language understanding and generation. In *ICML*, pages 12888–12900, 2022.
- [14] Junnan Li, Dongxu Li, Silvio Savarese, and Steven Hoi. Blip-2: Bootstrapping language-image pre-training with frozen image encoders and large language models. In *ICML*, pages 19730–19742, 2023.
- [15] Zhuang Liu, Hanzi Mao, Chao-Yuan Wu, Christoph Feichtenhofer, Trevor Darrell, and Saining Xie. A convnet for the 2020s. In *CVPR*, pages 11976–11986, 2022.
- [16] Lianmin Zheng, Wei-Lin Chiang, Ying Sheng, Siyuan Zhuang, Zhanghao Wu, Yonghao Zhuang, Zi Lin, Zhuohan Li, Dacheng Li, Eric Xing, et al. Judging llm-as-a-judge with mt-bench and chatbot arena. In *NeurIPS*, 2024.
- [17] Köpf Andreas, Vencu Richard, Coombes Theo, and Beaumont Romain. Laion coco: 600m synthetic captions from laion2b-en, 2022.
- [18] Christoph Schuhmann, Romain Beaumont, Richard Vencu, Cade Gordon, Ross Wightman, Mehdi Cherti, Theo Coombes, Aarush Katta, Clayton Mullis, Mitchell Wortsman, et al. Laion-5b: An open large-scale dataset for training next generation image-text models. In *NeurIPS*, pages 25278–25294, 2022.
- [19] Dan Hendrycks, Kevin Zhao, Steven Basart, Jacob Steinhardt, and Dawn Song. Natural adversarial examples. In *CVPR*, pages 15262–15271, 2021.
- [20] Dan Hendrycks, Steven Basart, Norman Mu, Saurav Kadavath, Frank Wang, Evan Dorundo, Rahul Desai, Tyler Zhu, Samyak Parajuli, Mike Guo, et al. The many faces of robustness: A critical analysis of out-of-distribution generalization. In *ICCV*, pages 8340–8349, 2021.
- [21] Benjamin Recht, Rebecca Roelofs, Ludwig Schmidt, and Vaishaal Shankar. Do imagenet classifiers generalize to imagenet? In *ICML*, pages 5389–5400, 2019.

- [22] Shilong Zhang, Peize Sun, Shoufa Chen, Min Xiao, Wenqi Shao, Wenwei Zhang, Kai Chen, and Ping Luo. Gpt4roi: Instruction tuning large language model on region-of-interest. *arXiv preprint arXiv:2307.03601*, 2023.
- [23] Zhiliang Peng, Wenhui Wang, Li Dong, Yaru Hao, Shaohan Huang, Shuming Ma, and Furu Wei. Kosmos-2: Grounding multimodal large language models to the world. *arXiv preprint arXiv:2306.14824*, 2023.
- [24] Jing Yu Koh, Daniel Fried, and Russ R Salakhutdinov. Generating images with multimodal language models. In *NeurIPS*, 2024.
- [25] Hugo Laurençon, Lucile Saulnier, Léo Tronchon, Stas Bekman, Amanpreet Singh, Anton Lozhkov, Thomas Wang, Siddharth Karamcheti, Alexander Rush, Douwe Kiela, et al. Obelics: An open web-scale filtered dataset of interleaved image-text documents. In *NeurIPS*, 2024.
- [26] Wanrong Zhu, Jack Hessel, Anas Awadalla, Samir Yitzhak Gadre, Jesse Dodge, Alex Fang, Youngjae Yu, Ludwig Schmidt, William Yang Wang, and Yejin Choi. Multimodal c4: An open, billion-scale corpus of images interleaved with text. In *NeurIPS*, 2024.
- [27] Yifan Li, Yifan Du, Kun Zhou, Jinpeng Wang, Wayne Xin Zhao, and Ji-Rong Wen. Evaluating object hallucination in large vision-language models. *arXiv preprint arXiv:2305.10355*, 2023.
- [28] Ao Zhang, Yuan Yao, Wei Ji, Zhiyuan Liu, and Tat-Seng Chua. Next-chat: An lmm for chat, detection and segmentation. *arXiv preprint arXiv: 2311.04498*, 2023.
- [29] Christoph Schuhmann, Richard Vencu, Romain Beaumont, Robert Kaczmarczyk, Clayton Mullis, Aarush Katta, Theo Coombes, Jenia Jitsev, and Aran Komatsuzaki. Laion-400m: Open dataset of clip-filtered 400 million image-text pairs. *arXiv preprint arXiv:2111.02114*, 2021.
- [30] Vicente Ordonez, Girish Kulkarni, and Tamara Berg. Im2text: Describing images using 1 million captioned photographs. In *NeurIPS*, 2011.
- [31] Soravit Changpinyo, Piyush Sharma, Nan Ding, and Radu Soricut. Conceptual 12m: Pushing web-scale image-text pre-training to recognize long-tail visual concepts. In *CVPR*, pages 3558–3568, 2021.
- [32] Xinlei Chen, Hao Fang, Tsung-Yi Lin, Ramakrishna Vedantam, Saurabh Gupta, Piotr Dollár, and C Lawrence Zitnick. Microsoft coco captions: Data collection and evaluation server. *arXiv preprint arXiv:1504.00325*, 2015.
- [33] Yash Goyal, Tejas Khot, Douglas Summers-Stay, Dhruv Batra, and Devi Parikh. Making the v in vqa matter: Elevating the role of image understanding in visual question answering. In *CVPR*, pages 6904–6913, 2017.
- [34] Oleksii Sidorov, Ronghang Hu, Marcus Rohrbach, and Amanpreet Singh. Textcaps: a dataset for image captioning with reading comprehension. In *ECCV*, pages 742–758, 2020.
- [35] Anand Mishra, Shashank Shekhar, Ajeet Kumar Singh, and Anirban Chakraborty. Ocr-vqa: Visual question answering by reading text in images. In *ICDAR*, pages 947–952, 2019.
- [36] Drew A Hudson and Christopher D Manning. Gqa: A new dataset for real-world visual reasoning and compositional question answering. In *CVPR*, pages 6700–6709, 2019.
- [37] Kenneth Marino, Mohammad Rastegari, Ali Farhadi, and Roozbeh Mottaghi. Ok-vqa: A visual question answering benchmark requiring external knowledge. In *CVPR*, pages 3195–3204, 2019.
- [38] Amanpreet Singh, Vivek Natarajan, Meet Shah, Yu Jiang, Xinlei Chen, Dhruv Batra, Devi Parikh, and Marcus Rohrbach. Towards vqa models that can read. In *CVPR*, pages 8317–8326, 2019.
- [39] Dustin Schwenk, Apoorv Khandelwal, Christopher Clark, Kenneth Marino, and Roozbeh Mottaghi. A-okvqa: A benchmark for visual question answering using world knowledge. In *ECCV*, pages 146–162, 2022.
- [40] Sahar Kazemzadeh, Vicente Ordonez, Mark Matten, and Tamara Berg. Referitgame: Referring to objects in photographs of natural scenes. In *EMNLP*, pages 787–798, 2014.
- [41] Junhua Mao, Jonathan Huang, Alexander Toshev, Oana Camburu, Alan L Yuille, and Kevin Murphy. Generation and comprehension of unambiguous object descriptions. In *CVPR*, pages 11–20, 2016.
- [42] Xianjie Chen, Roozbeh Mottaghi, Xiaobai Liu, Sanja Fidler, Raquel Urtasun, and Alan Yuille. Detect what you can: Detecting and representing objects using holistic models and body parts. In *CVPR*, pages 1971–1978, 2014.
- [43] Ju He, Shuo Yang, Shaokang Yang, Adam Kortylewski, Xiaoding Yuan, Jie-Neng Chen, Shuai Liu, Cheng Yang, Qihang Yu, and Alan Yuille. Partimagenet: A large, high-quality dataset of parts. In *ECCV*, pages 128–145, 2022.
- [44] Rowan Zellers, Yonatan Bisk, Ali Farhadi, and Yejin Choi. From recognition to cognition: Visual commonsense reasoning. In *CVPR*, pages 6720–6731, 2019.

- [45] Ranjay Krishna, Yuke Zhu, Oliver Groth, Justin Johnson, Kenji Hata, Joshua Kravitz, Stephanie Chen, Yannis Kalantidis, Li-Jia Li, David A Shamma, et al. Visual genome: Connecting language and vision using crowd-sourced dense image annotations. *International Journal of Computer Vision*, 123:32–73, 2017.
- [46] Jonathan Krause, Justin Johnson, Ranjay Krishna, and Li Fei-Fei. A hierarchical approach for generating descriptive image paragraphs. In *CVPR*, pages 317–325, 2017.
- [47] Danna Gurari, Qing Li, Abigale J Stangl, Anhong Guo, Chi Lin, Kristen Grauman, Jiebo Luo, and Jeffrey P Bigham. Vizwiz grand challenge: Answering visual questions from blind people. In *CVPR*, pages 3608–3617, 2018.
- [48] Abhishek Das, Satwik Kottur, Khushi Gupta, Avi Singh, Deshraj Yadav, José MF Moura, Devi Parikh, and Dhruv Batra. Visual dialog. In *CVPR*, pages 326–335, 2017.
- [49] IDEFICS. Introducing idefics: An open reproduction of state-of-the-art visual language model. <https://huggingface.co/blog/idefics>, 2023.
- [50] Shaohan Huang, Li Dong, Wenhui Wang, Yaru Hao, Saksham Singhal, Shuming Ma, Tengchao Lv, Lei Cui, Owais Khan Mohammed, Barun Patra, et al. Language is not all you need: Aligning perception with language models. In *NeurIPS*, 2024.
- [51] Jiabo Ye, Anwen Hu, Haiyang Xu, Qinghao Ye, Ming Yan, Yuhao Dan, Chenlin Zhao, Guohai Xu, Chenliang Li, Junfeng Tian, et al. mplug-docowl: Modularized multimodal large language model for document understanding. *arXiv preprint arXiv:2307.02499*, 2023.
- [52] Haotian Liu, Chunyuan Li, Yuheng Li, and Yong Jae Lee. Improved baselines with visual instruction tuning. *arXiv preprint arXiv:2310.03744*, 2023.
- [53] Jinze Bai, Shuai Bai, Shusheng Yang, Shijie Wang, Sinan Tan, Peng Wang, Junyang Lin, Chang Zhou, and Jingren Zhou. Qwen-vl: A frontier large vision-language model with versatile abilities. *arXiv preprint arXiv:2308.12966*, 2023.
- [54] Quan Sun, Yufeng Cui, Xiaosong Zhang, Fan Zhang, Qiyang Yu, Zhengxiong Luo, Yueze Wang, Yongming Rao, Jingjing Liu, Tiejun Huang, et al. Generative multimodal models are in-context learners. *arXiv preprint arXiv:2312.13286*, 2023.
- [55] Jialian Wu, Jianfeng Wang, Zhengyuan Yang, Zhe Gan, Zicheng Liu, Junsong Yuan, and Lijuan Wang. Grit: A generative region-to-text transformer for object understanding. *arXiv preprint arXiv:2212.00280*, 2022.
- [56] Aditya Ramesh, Mikhail Pavlov, Gabriel Goh, Scott Gray, Chelsea Voss, Alec Radford, Mark Chen, and Ilya Sutskever. Zero-shot text-to-image generation. In *ICML*, pages 8821–8831, 2021.
- [57] Ming Ding, Zhuoyi Yang, Wenyi Hong, Wendi Zheng, Chang Zhou, Da Yin, Junyang Lin, Xu Zou, Zhou Shao, Hongxia Yang, et al. Cogview: Mastering text-to-image generation via transformers. In *NeurIPS*, pages 19822–19835, 2021.
- [58] Ming Ding, Wendi Zheng, Wenyi Hong, and Jie Tang. Cogview2: Faster and better text-to-image generation via hierarchical transformers. In *NeurIPS*, pages 16890–16902, 2022.
- [59] Alex Nichol, Prafulla Dhariwal, Aditya Ramesh, Pranav Shyam, Pamela Mishkin, Bob McGrew, Ilya Sutskever, and Mark Chen. Glide: Towards photorealistic image generation and editing with text-guided diffusion models. *arXiv preprint arXiv:2112.10741*, 2021.
- [60] Oran Gafni, Adam Polyak, Oron Ashual, Shelly Sheynin, Devi Parikh, and Yaniv Taigman. Make-a-scene: Scene-based text-to-image generation with human priors. In *ECCV*, pages 89–106, 2022.
- [61] Aditya Ramesh, Prafulla Dhariwal, Alex Nichol, Casey Chu, and Mark Chen. Hierarchical text-conditional image generation with clip latents. *arXiv preprint arXiv:2204.06125*, 2022.
- [62] Yinfei Yang, Daniel Cer, Amin Ahmad, Mandy Guo, Jax Law, Noah Constant, Gustavo Hernandez Abrego, Steve Yuan, Chris Tar, Yun-Hsuan Sung, et al. Multilingual universal sentence encoder for semantic retrieval. *arXiv preprint arXiv:1907.04307*, 2019.
- [63] Chitwan Saharia, William Chan, Saurabh Saxena, Lala Li, Jay Whang, Emily L Denton, Kamyar Ghasemipour, Raphael Gontijo Lopes, Burcu Karagol Ayan, Tim Salimans, et al. Photorealistic text-to-image diffusion models with deep language understanding. In *NeurIPS*, pages 36479–36494, 2022.
- [64] Jiahui Yu, Yuanzhong Xu, Jing Yu Koh, Thang Luong, Gunjan Baid, Zirui Wang, Vijay Vasudevan, Alexander Ku, Yinfei Yang, Burcu Karagol Ayan, et al. Scaling autoregressive models for content-rich text-to-image generation. *arXiv preprint arXiv:2206.10789*, 2(3):5, 2022.

- [65] Armen Aghajanyan, Bernie Huang, Candace Ross, Vladimir Karpukhin, Hu Xu, Naman Goyal, Dmytro Okhonko, Mandar Joshi, Gargi Ghosh, Mike Lewis, et al. Cm3: A causal masked multimodal model of the internet. *arXiv preprint arXiv:2201.07520*, 2022.
- [66] Ramakrishna Vedantam, C Lawrence Zitnick, and Devi Parikh. Cider: Consensus-based image description evaluation. In *CVPR*, pages 4566–4575, 2015.
- [67] Tsung-Yi Lin, Michael Maire, Serge Belongie, James Hays, Pietro Perona, Deva Ramanan, Piotr Dollár, and C Lawrence Zitnick. Microsoft coco: Common objects in context. In *ECCV*, pages 740–755, 2014.
- [68] Jordi Pont-Tuset, Jasper Uijlings, Soravit Changpinyo, Radu Soricut, and Vittorio Ferrari. Connecting vision and language with localized narratives. In *ECCV*, pages 647–664, 2020.
- [69] Martin Heusel, Hubert Ramsauer, Thomas Unterthiner, Bernhard Nessler, and Sepp Hochreiter. Gans trained by a two time-scale update rule converge to a local nash equilibrium. In *NeurIPS*, 2017.
- [70] Stanislaw Antol, Aishwarya Agrawal, Jiasen Lu, Margaret Mitchell, Dhruv Batra, C Lawrence Zitnick, and Devi Parikh. Vqa: Visual question answering. In *ICCV*, pages 2425–2433, 2015.

## Contents

<b>1</b>	<b>Introduction</b>	<b>2</b>
<b>2</b>	<b>Related Work</b>	<b>3</b>
2.1	LMM for Text Generation Only . . . . .	3
2.2	LMM for Image and Text Generation . . . . .	3
<b>3</b>	<b>Method</b>	<b>4</b>
3.1	Architecture . . . . .	4
3.2	Pipeline . . . . .	5
3.3	Training and Inference . . . . .	5
<b>4</b>	<b>Experiment</b>	<b>6</b>
4.1	Implementation Details . . . . .	6
4.2	Experimental Results . . . . .	7
4.3	Ablation Study . . . . .	8
<b>5</b>	<b>Conclusion</b>	<b>9</b>
<b>A</b>	<b>Limitation</b>	<b>15</b>
<b>B</b>	<b>Broader Impacts</b>	<b>15</b>
<b>C</b>	<b>Additional Ablation Study</b>	<b>15</b>
C.1	Ablation Study of Input Image Resolution . . . . .	15
C.2	Ablation Study of Coefficient $\lambda$ . . . . .	15
C.3	Ablation Study of Training Recipes . . . . .	15
<b>D</b>	<b>Additional Implementation Details</b>	<b>15</b>
D.1	Dataset Construction . . . . .	15
D.2	Image-Text Alignment Pre-training . . . . .	16
D.3	Image-Text Instruction Fine-tuning . . . . .	16
D.4	Mask-Text Instruction Fine-tuning . . . . .	16
D.5	Evaluation . . . . .	17
<b>E</b>	<b>Additional Visualization Examples</b>	<b>17</b>
E.1	Consistency Semantic Image Synthesis . . . . .	17
E.2	Text Condition Image Synthesis . . . . .	17
E.3	Robustness Comparison . . . . .	17
E.4	Image-Text Multimodal Dialogue . . . . .	18
E.5	Mask-Text Multimodal Dialogue . . . . .	18

## A Limitation

Although our method significantly enhances the visual robustness of interleaved image-text modeling multimodal models after image-text alignment pre-training, it, unfortunately, cannot eliminate but only alleviate the robustness knowledge forgetting issue caused by subsequent fine-tuning, as shown in the Table 1 and Table 6. Additionally, our model requires using a diffusion model as another eye to correct and update the erroneous knowledge of the image encoder to improve the overall visual robustness of the multimodal model. However, updating larger image encoders such as CLIP-ViT-L and CLIP-ViT-G[11] will increase the training overhead, which may limit the application of our model. We hope that in the future, the diffusion model can completely replace the image encoder to further enhance the effectiveness of our method.

## B Broader Impacts

The proposed method introduces a novel strategy to enhance the robustness and generalization capabilities of multimodal models by leveraging a diffusion model as an additional eye for large language models. This strategy allows for the correction and updating of potential semantic errors in the image encoder, leading to significant improvements in handling out-of-distribution data and mitigating visual hallucinations. Overall, our contributions provide a significant step forward in the field of multimodal, offering a robust, efficient, and scalable solution for improving the accuracy and reliability of multimodal models. The broader impacts of this work include the potential for more intelligent and adaptive AI systems that can operate effectively in diverse and challenging environments.

## C Additional Ablation Study

we provide more ablation studies for DEEM in this section, all of which share the same settings. All the code, models, and data tools will be released soon.

### C.1 Ablation Study of Input Image Resolution

In addition to the aforementioned exploration, we also scale up the input image resolution for performance gain. The performance gain becomes larger when further increasing the input image resolution from 256 to 448 in image-text instruction fine-tuning, as shown in Table 8. Such results indicate our method could better exploit the additional information gained from high resolution.

Table 8: Ablation study of input image resolution in image-text instruction fine-tuning with 2k training steps and 16 batch size.

resolution	RVQA-A	RVQA-R	RVQA-V	POPE-R	POPE-P	POE-A	OK-VQA
256	51.5	<b>59.1</b>	57.9	85.9	77.1	76.4	38.7
448	<b>52.5</b>	57.6	<b>58.1</b>	<b>86.0</b>	<b>79.2</b>	<b>77.1</b>	<b>41.0</b>

### C.2 Ablation Study of Coefficient $\lambda$

Moreover, we conduct an ablation study on coefficient  $\lambda$  in loss function. As shown in Table 9, setting  $\lambda = 5$  achieves a better balance between robustness and hallucination empirically.

### C.3 Ablation Study of Training Recipes

We also conduct an ablation study to control the trainability of different training modules. As shown in Table 10, we found that freezing the DM (Diffusion Model) while not freezing the VFM (Visual Foundation Model) during training yields the best robustness and hallucination results.

## D Additional Implementation Details

### D.1 Dataset Construction

As shown in Fig. 5, we first convert the original ImageNet-A [19], ImageNet-R [20], and ImageNet-V2 [21] data into a VQA format that the multimodal model can evaluate. Specifically, we use the CLIP-ViT-L model for hard example mining, predicting the incorrect category la-

Table 9: Ablation study of coefficient  $\lambda$  in image-text alignment pre-training with 2k training steps and 16 batch size.

$\lambda$	RVQA-A	RVQA-R	RVQA-V	POPE-R	POPE-P	POE-A	OK-VQA
1	51.6	52.0	49.6	48.5	50.0	50.0	18.9
5	<b>51.9</b>	<b>54.3</b>	<b>52.7</b>	48.4	50.1	50.0	<b>20.7</b>
10	51.7	52.7	51.9	<b>48.7</b>	<b>50.3</b>	<b>50.3</b>	20.1

bel with the highest confidence score apart from the ground truth category label. We then use a pre-defined prompt as: “Is [category label] the main object in this image? Please answer yes or no.” to simultaneously construct a pair of positive and negative example samples, allowing the model to answer “yes” or “no”. By using this design, we can evaluate the robustness of multimodal models in an unbiased manner with the new benchmark called RobustVQA, facilitating both assessment and comparison.

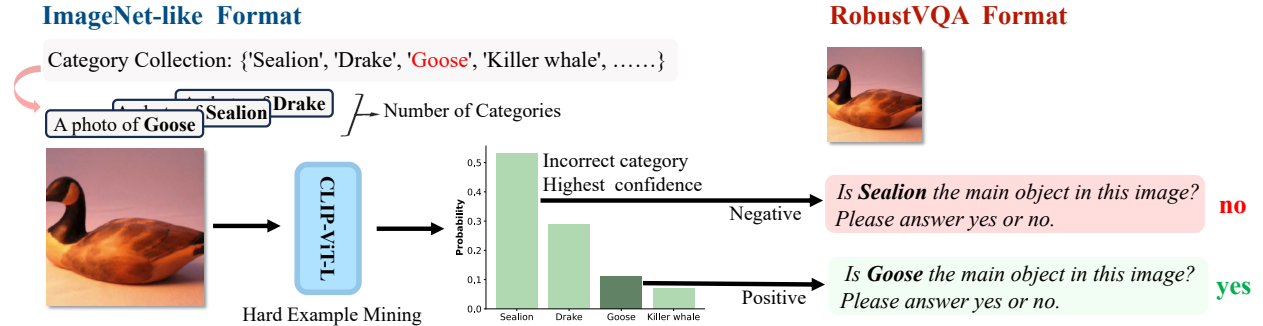


Figure 5: **Robustness dataset construction process.** We use the CLIP-ViT-L model for hard example mining and then transform them into question-answer pairs via a pre-defined template.

## D.2 Image-Text Alignment Pre-training

We use MMC4-Core [26], LAION-400M [29], SBU [30], and CC-12M [31] as the pre-training dataset. For LAION-400M [29], SBU [30], and CC-12M [31], instead of utilizing the original annotations, we use the version filtered by the pre-trained BLIP-2 model [14]. For simplicity, we refer to it as BLIP-LCS hereafter. “LCS” abbreviates the LAION, CC, and SBU datasets. Text prompts with lengths shorter than 10 are also filtered out. Due to network constraints, we only collect approximately 6M of MMC4-Core and 20M of BLIP-LCS data. The sampling probability of MMC4 is twice that of BLIP-LCS. The images are inserted before or after the corresponding text sentence with equal probability. Specifically, images with a CLIP similarity score below 0.24 will be discarded, and only 6 images at most will be kept for each document in MMC4-Core. We also exclude 100% of all documents that do not contain any images, and 50% of documents that contain only 1 image. For image-text-pair BLIP-LCS datasets, we randomly sample multiple image-text pairs from the same dataset and concatenate them to the maximum context length (*i.e.*, 2048) during pre-training. For interleaved image and text MMC4-Core [26] datasets, we also split and concatenate the documents to form the training samples. Such a concatenation strategy can utilize the full context window of Large Language Models and thus achieve high data efficiency. Besides that, for image generation, we ignore the training loss of images which are the first element in the sequence. The text condition of the rest images is dropped with a 10% probability to improve classifier-free guidance sampling. The detailed hyper-parameters of image-text alignment pre-training are listed in Table 11.

Table 10: Ablation study of training recipe in image-text alignment pre-training with 10k training steps and 128 batch size.

VFM	DM	RVQA-A	RVQA-R	RVQA-V	POPE-R	POPE-P	POPE-A
freeze	unfreeze	53.2	56.1	54.7	50.6	52.0	51.9
unfreeze	freeze	<b>56.8</b>	<b>68.6</b>	<b>63.1</b>	<b>69.9</b>	<b>70.3</b>	<b>68.9</b>
unfreeze	unfreeze	50.3	52.5	53.1	54.8	56.3	56.1

## D.3 Image-Text Instruction Fine-tuning

We utilize public available datasets for supervised fine-tuning, including LLaVA-665K[1], COCO Caption [32], VQAv2 [33], TextCaps [34], OCR-VQA [35], GQA [36], OK-VQA [37], TextVQA [38], and AOK-VQA [39]. We use the following prompt template “Based on the image, please answer the question. {image} {question}. The answer is: {answer} ” to convert the data into a mixture of instruction following forms, resulting in approximately 800K instruction data for the second-stage image-text instruction fine-tuning. The detailed hyper-parameters of image-text instruction fine-tuning are listed in Table 11.

## D.4 Mask-Text Instruction Fine-tuning

We collect short text and pixel-level mask pairs from the publicly available object-level datasets (COCO, RefCOCO, RefCOCO+) and part-level datasets (Pascal Part, Part Imagenet), then transform them into instruction following data. Moreover, Visual Genome (VG) and Visual Commonsense Reasoning (VCR) datasets are employed to add more



multiple region understanding data, resulting in approximately 200K instruction data for the third-stage mask-text instruction fine-tuning. See more hyper-parameters details in Table 11.

## D.5 Evaluation

As shown in Fig. 6, DEEM achieves the best results on both hallucination and robustness benchmarks even at the smallest scale, demonstrating the efficiency and effectiveness of our approach. In addition to visual robustness and hallucination, we also use various benchmarks and datasets, such as image caption, visual question answering, text-to-image generation and so on, to assess the image-text comprehension capabilities. All these evaluation tasks and metrics are listed in Table 12. The prompt templates for each task are listed in Fig. 8.

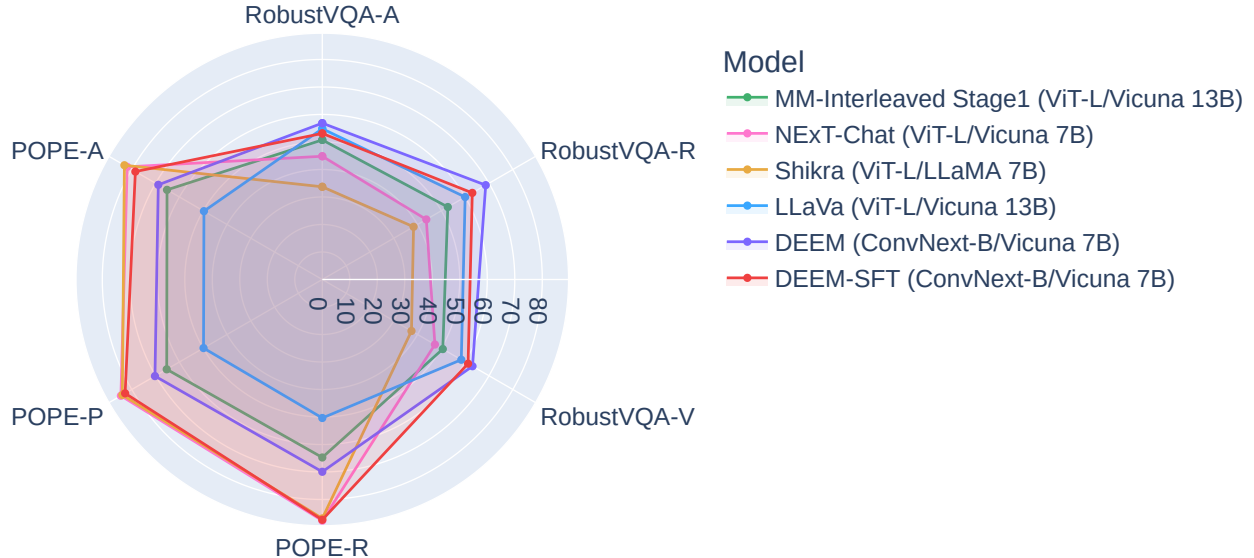


Figure 6: **Performance on visual robustness and hallucination benchmark.** DEEM achieves the best results on robustness benchmark and competitive performance on hallucination even at the smallest scale, demonstrating the efficiency and effectiveness of our approach.

## E Additional Visualization Examples

### E.1 Consistency Semantic Image Synthesis

We visualize some consistency semantic image synthesis and display both the original images and their reconstructed versions in Fig. 10. DEEM accurately recovers the features of the original images without causing distortion.

### E.2 Text Condition Image Synthesis

In Fig. 9, we present some text-to-image synthesis examples from DEEM, demonstrating its capability to generate corresponding images based on given prompts.

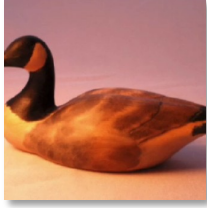
### E.3 Robustness Comparison

In Fig. 7, we present a comparative analysis of visual robustness results between our model, DEEM, and other state-of-the-art models: LLaVA [1], NeXt-Chat [28], and MM-Interleaved [9]. When encountering natural adversarial samples or out-of-distribution samples, the image encoder in their models will output incorrect semantic information, leading to incorrect category answers. In contrast, our method uses a diffusion model as the eyes of the large language model to inspect and correct the output features of the image encoder. This process eliminates incorrect semantic outputs from the image encoder, ultimately allowing the large language model to produce the correct category answer. This simple yet effective approach significantly enhances the model’s robustness and generalization capabilities.

---

**Visual input example, Goose:**


---



User	Based on the image, please answer the question. What is the main object in this image? Chose from the list: ['Sealion', 'Drake', 'Goose', 'Killer whale']. Let's think step by step.
DEEM (Ours)	A carved goose sitting on a flat surface. So the answer is goose ✓
LLaVA	The main object in this image is a drake. ✗
NeXT-Chat	A sculpture of a duck sitting on a table. So the answer is duck. ✗
MM-Interleaved	Sealion ✗

Figure 7: **Case Comparison.** Compared to other SOTA models, including LLaVa, NeXT-Chat, and MM-Interleaved, when encountering out-of-distribution data, their models are affected by incorrect semantics from the image encoder and cannot output the correct answer. However, DEEMcan output the correct answer via generative feedback.

#### E.4 Image-Text Multimodal Dialogue

In Fig. 11, we show the image-text dialogue case examples of DEEM. Our model can input any interleaved layout of text-image data and simultaneously understand and generate text-image outputs in any interleaved layout, representing the future of next-generation multimodal dialogue.

#### E.5 Mask-Text Multimodal Dialogue

In addition to image-level input, DEEMalso supports mask-text input to perform fine-grained region-level reasoning tasks. As shown in the Fig. 12, DEEMcan accurately extract region semantics of the image based on the input mask and complete the corresponding instruction tasks.

Table 11: **Training recipes** for DEEM. The three training stages are introduced in Section 3.3. Stage I: Image-Text Alignment Pre-training, Stage II: Image-Text Instruction Fine-tuning, Stage III: Mask-Text Instruction Fine-tuning.

	Stage I	Stage II	Stage III
Phase	Image-Text Alignment	Image-Text SFT	Mask-Text SFT
<i>Training Hyper-Parameters</i>			
Input image resolution	256×256	448×448	448×448
Output image resolution	512×512	512×512	512×512
VFM	CLIP-ConvNext-B	CLIP-ConvNext-B	CLIP-ConvNext-B
LLM	Vicuna-7B v1.5	Vicuna-7B v1.5	Vicuna-7B v1.5
DM	Stable Diffusion v2.1	Stable Diffusion v2.1	Stable Diffusion v2.1
$\lambda$	5	5	5
Learning Rate	2e-5 (image encoder&decoder) 1e-4 (others)	1e-6 (language model) 1e-5 (others)	1e-6 (language model) 1e-5 (others)
Optimizer	AdamW	AdamW	AdamW
Optimizer hyper-parameters	$\beta_1, \beta_2, \epsilon = 0.9, 0.995, 1e-6$	$\beta_1, \beta_2, \epsilon = 0.9, 0.999, 1e-8$	$\beta_1, \beta_2, \epsilon = 0.9, 0.999, 1e-8$
Weight Decay	0.05	0.05	0.05
Training iterations	10k	10k	10k
Warmup steps	1k	500	500
Learning Rate Scheduler	Cosine	Cosine	Cosine
Batch Size Per GPU	4	16	2
Maximum Token Length	2048	2048	2048
Augmentation	CenterCrop	-	-
Unfreeze LLM	✗	✓	✓
Unfreeze DM	✗	✗	✗
Unfreeze VFM	✓	✗	✗
<i>Training Data</i>			
Dataset	① MMC4 ② BLIP-LCS	① LLaVA-Mix-665K ② VQA-Mixture ③ COCO Caption	① COCO/ReferCOCO/ReferCOCO+ ② Pascal-Part/Part-ImageNet ④ VG/VRC
Data Size	~26M	~800K	~200K
Data Type	Interleave/Pair	Instruction	Instruction
<i>Training Cost</i>			
GPU Device	32×NVIDIA A100	32×NVIDIA A100	32×NVIDIA A100
Training Time	~30h	~6h	~3h

Table 12: **Overall descriptions of the evaluation benchmarks** for evaluating capabilities, including image-level captioning, image-level visual question answering, text-to-image generation, region-level image captioning, visual robustness, and hallucination.

	Dataset	Task description	Eval Split	Metric
CAP.	COCO [32]	Scene description	test	CIDEr(↑) [66]
	Image2Paragraph [46]	Scene description	test	CIDEr(↑) [66]
VQA.	VQAv2 [33]	Scene understanding QA	test-dev	VQA Acc(↑) [70]
	OKVQA [37]	External knowledge QA	val	VQA Acc(↑) [70]
	GQA [36]	Scene understanding QA	test-dev	VQA Acc(↑) [70]
	VizWiz [47]	Scene understanding QA	test-dev	VQA Acc(↑) [70]
	VisDial [48]	Image dialogue	val	NDCG(↑)
SYN.	MS-COCO [67]	Text-Conditional Image Synthesis	val-30K	FID(↓) [69]
	LN-COCO [68]	Text-Conditional Image Synthesis	val	FID(↓) [69]
REF.	RefCOCO [40]	Region-level scene description	val	CIDEr(↑) [66]
	RefCOCO+ [41]	Region-level scene description	val	CIDEr(↑) [66]
	RefCOCOfg [41]	Region-level scene description	val	CIDEr(↑) [66]
OOD.	RobustVQA-V	Out-of-Distribution Robustness	val	Acc(↑)
	RobustVQA-R	Out-of-Distribution Robustness	val	Acc(↑)
	RobustVQA-A	Out-of-Distribution Robustness	val	Acc(↑)
OOD.	POPE-R [27]	Visual Hallucination	val	Acc(↑)
	POPE-P [27]	Visual Hallucination	val	Acc(↑)
	POPE-A [27]	Visual Hallucination	val	Acc(↑)

---

System Prompt	
<b>You are a helpful assistant.</b>	
-----	
(a) VQA	
USER:	<b>Based on the image, please answer the question.</b> {IMAGE} {QUESTION} Please provide an accurate answer within one word.
ASSISTANT:	The answer is <ANSWER>
-----	
(b) Image Captioning	
USER:	{IMAGE} Could you provide a short description of the image?
ASSISTANT:	A photo of <ANSWER>
-----	
(c) Referring	
USER:	{IMAGE} Provide a short description for this <ref>region1</ref> {MASK}
ASSISTANT:	<ANSWER>
-----	
(d) Hallucination	
USER:	<b>Based on the image, please answer the question.</b> {IMAGE} Is there a <OBJECT> in the image? Please answer yes or no.
ASSISTANT:	The answer is <ANSWER>
-----	
(e) Robustness	
USER:	<b>Based on the image, please answer the question.</b> {IMAGE} Is <OBJECT> the main object in this image? Please answer yes or no.
ASSISTANT:	The answer is <ANSWER>

---

Figure 8: **Prompt template used for evaluation.** (a) VQA includes VQAv2, VizWiz, OKVQA, GQA, and VisDial. (b) Image Captioning includes COCO, Image2Paragraph. (c) Region-level Image Captioning includes RefCOCOg. (d) Visual hallucination includes POPE. (e) Visual Robustness includes RobustVQA-A, RobustVQA-R, and RobustVQA-V.  $\mathcal{I}_{\text{IMAGE}}_i$  denotes the input image representation,  $\mathcal{I}_{\text{MASK}}_i$  denotes the mask-level image representation,  $\mathcal{I}_{\text{QUESTION}}_i$  denotes each specific question,  $\mathcal{I}_{\text{ANSWER}}_i$  is the generated answer, and  $\mathcal{I}_{\text{OBJECT}}_i$  is the specific object name in a question of POPE and RobustVQA.



Figure 9: **image-to-image generation examples with the outputs of image encoder.** (a,c,e) are original images and (b,d,f) are synthesis images based on the image embedding<sub>23</sub> of original images.



*Small bird with a pale yellow underside light brown crown and back gray tail and wing tips tip of tail feather bright yellow black eyes and black strip over eyes*



*An armchair in the shape of an avocad*

*A couple of glasses are sitting on a tabl*



*A long wooden bench in front of a brick wall*



*Downtown Beijing at sunrise. detailed ink wash*

*A beat-up truck in the desert*

Figure 10: **Text-to-image generation examples with prompts.** DEEMcan generate vivid images based on input text conditions.

Photograph A:



Photograph B:



What is written in photo A and B? What is the difference between these two photos? Answer in detail about the difference in written words and styles.



In Photograph A, the word "DEEM" is written on a pink background with hearts placed around it. This creates an eye-catching and unique display for this particular image of roses against another colorful rose patterned backdrop that complements DEEM's bright colors. On the other hand, in Photograph B, the same words are displayed using vintage typography style and printed over a light blue gradient. The overall effect looks more nostalgic or dreamy compared to Photograph A but has similar visual elements such as flowers arranged beneath DEEM. These differences highlight how design choices can impact mood and perception while retaining essential components like textual content.

help me mix the styles of the above two images to create a new image that combines both modern and romantic styles featuring the word "DEEM":



This image merges the sleek, contemporary elements with soft, pastel romantic touches, creating a unique blend of both aesthetics.





Figure 12: **Examples of mask-text multimodal dialogue** between human and DEEM. Text and mask can be used as inputs and DEEM outputs the corresponding answer, and multi-round dialogue is shown.